

MuSACo: Multimodal Subject-Specific Selection and Adaptation for Expression Recognition with Co-Training

Muhammad Osama Zeeshan¹, Natacha Gillet², Alessandro Lameiras Koerich¹, Marco Pedersoli¹, Francois Bremond³, Eric Granger¹

¹ LIVIA, Dept. of Systems Engineering, ETS Montreal, Canada

² École Polytechnique, Palaiseau, France

³ Inria, 2004 Rte des Lucioles, Valbonne 06902, France
muhammad-osama.zeeshan.1@ens.etsmtl.ca, eric.granger@etsmtl.ca

Abstract

Personalized expression recognition (ER) involves adapting a machine learning model to subject-specific data for improved recognition of expressions with considerable inter-personal variability. Subject-specific ER can benefit significantly from multi-source domain adaptation (MSDA) methods – where each domain corresponds to a specific subject – to improve model accuracy and robustness. Despite promising results, state-of-the-art MSDA approaches often overlook multimodal information or blend sources into a single domain, limiting subject diversity and failing to explicitly capture unique subject-specific characteristics. To address these limitations, we introduce MuSACo, a multimodal subject-specific selection and adaptation method for ER based on co-training. It leverages complementary information across multiple modalities and multiple source domains for subject-specific adaptation. This makes MuSACo particularly relevant for affective computing applications in digital health, such as patient-specific assessment for stress or pain, where subject-level nuances are crucial. MuSACo selects source subjects relevant to the target and generates pseudo-labels using the dominant modality for class-aware learning, in conjunction with a class-agnostic loss to learn from less confident target samples. Finally, source features from each modality are aligned, while only confident target features are combined. Our experimental results¹ on challenging multimodal ER datasets – BioVid and StressID – show that MuSACo can outperform UDA (blending) and state-of-the-art MSDA methods.

1. Introduction

Expression recognition (ER) has achieved significant success in computer vision due to its relevance in numer-

ous real-world applications, such as pain estimation, stress monitoring, and affective computing [1, 2, 18, 32, 37]. These models can achieve a high level of performance under supervised settings or when provided with limited labeled data [25, 27]. However, their effectiveness mainly depends on the availability of annotated datasets, which are difficult to obtain, and often fail to generalize for subtle expressions and across diverse individuals due to variations in cultural, environmental, and individual expressiveness [13]. Unsupervised domain adaptation (UDA) [10, 20, 43] has emerged as a promising direction to address this challenge by adapting a model from a labeled source domain to an unlabeled target domain. In the context of ER, this facilitates personalization, where a model trained on labeled expression data from multiple source subjects is adapted to a new, unlabeled target subject. While existing UDA approaches [11, 18, 49] adapt to the unlabeled target dataset treated as a domain by either using single or blended labeled source subjects, recent advances in multi-source domain adaptation (MSDA) [45, 46] leverages information from multiple source subjects (domains). This encourages diversity in the source model for adaptation to an unlabeled target subject (domain). This method facilitates more precise and targeted adaptation strategies for developing a personalized ER model (see Fig. 1(a)).

Despite these advances, the majority of subject-specific ER approaches are predominantly constrained to a single modality [11, 46]. However, human expressions and fine-grained affective cues are often difficult to capture reliably from a single modality alone [19, 47]. To address this limitation, we focus on a multimodal setting that leverages the complementary strengths of multimodal data. Multimodal ER (MER) has been widely studied in the literature [1, 2, 26, 34], typically outperforming unimodal systems by leveraging complementary information from multiple modalities. MER approaches integrate diversity from various modalities, such as visual, textual, audio, or physiolog-

¹Our code is provided in suppl. materials and will be made public.

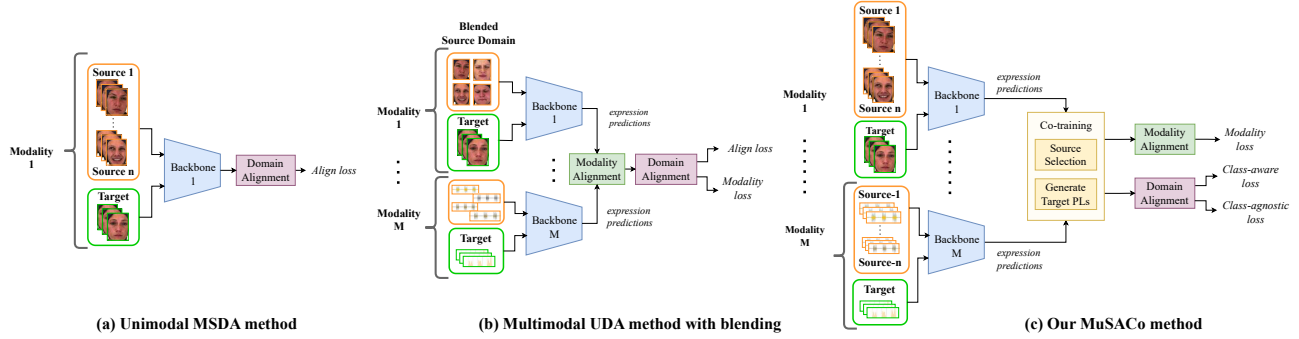


Figure 1. Comparison of MuSACo against unimodal MSDA and multimodal UDA (blending) ER methods for subject-based adaptation. **(a) Unimodal MSDA** aligns multiple source subjects to the target within a single modality, which reduces its accuracy. **(b) Multimodal UDA with blending** incorporates single or blended source domains for target adaptation but does not fully exploit multiple subject-specific diversity. **(c) MuSACo** selects relevant sources per modality using co-training, and aligns them to the target using both class-aware and class-agnostic losses before fusing modalities for final prediction.

ical signals [7] to enhance model performance. In subject-based ER, most MER methods focus on fully or weakly labeled data [26, 34], hindering the ability of the model to have a better adaptation to unlabeled data. Nevertheless, there are some studies [15, 39] that introduced multiple modalities, specifically for EEG. Eye movement signals with a single source or combine multiple sources into a single domain (see Fig. 1(b)). Their reliance on a single source often fails to provide diversity in source domains. Furthermore, blending multiple sources into a single domain [16] cannot explicitly capture the unique subject-specific characteristics of each source subject, which is crucial for subject-specific target adaptation.

In this paper, we propose MuSACo, a novel approach for Multimodal Subject-Specific Selection and Adaptation for ER using Co-Training in an MSDA setting (Fig. 1(c)). Our method exploits the complementary information from multiple modalities while selecting the most relevant source subjects for the target. It takes advantage of the unique characteristics of each subject for better performance on the target subject (domain²). There are two key challenges when considering multiple modalities for subject-specific MSDA: (1) effectively leveraging multiple source subject information within multimodal systems, and (2) achieving cross-domain and cross-modal alignment.

To address the first challenge, we propose the *selection of source subjects* most relevant to the target subject. While prior work [45] has shown that selecting source subjects based on their relevance to the target improves adaptation, it relies solely on a single modality to guide the source selection process. In this paper, we propose a co-training-based strategy for selecting source subjects that leverage multiple modalities, as different modalities complement each other by providing unique characteristics from various perspec-

tives. Thus, selecting sources using co-training benefits the adaptation process. Furthermore, to improve generalization across individuals, we encourage the model to focus on expression-specific features by disentangling identity-related information during source training.

For the second challenge, we first focus on cross-domain alignment. State-of-the-art MSDA methods [17, 30] highlight the effectiveness of class-aware alignment in bridging dissimilar distributions. This typically involves generating pseudo-labels (PLs) for the target subject. In our proposed method, we extend this by leveraging co-training for the *generation of target PLs*. Specifically, PLs for unlabeled target data are generated by selecting predictions from the dominant modality (e.g., visual or physiological), chosen by their probability score and threshold. This ensures diversity in modality-specific feature representations and captures complementary aspects of the data. These PLs then guide class-aware alignment between source and target subjects, minimizing distribution mismatch. Although PLs allow improving the model performance, they heavily depend on the choice of a threshold to filter out unreliable samples. In particular, high threshold values ensure the sample quality. While setting a high threshold value often results in discarding potentially useful but less confident samples. To mitigate this, we introduce a class-agnostic loss that aligns non-confident target samples with the source. This encourages the unreliable samples to contribute to the learning process to improve the robustness of the model. For modality alignment, including a fusion module [1, 26] has proven to enhance MER performance. In MuSACo, a fusion module is added to concatenate features from different modalities for each selected source subject. For the target, only reliable samples (selected via co-training) are combined.

The contributions of this paper are summarized as follows. **(1) MuSACo**: a novel multimodal MSDA method

²The terms domain and subject are used interchangeably.

for accurate subject specific adaptation. It selects relevant source subjects from the target using co-training, leveraging complementary information across modalities. (2) An effective alignment process that relies on co-training to generate confident target PLs for class-aware loss, combined with class-agnostic loss to handle non-confident target samples. (3) Extensive experiments performed on challenging MER datasets (BioVid and StressID) shows the efficacy of MuSACo. It can outperform the UDA (blending) and state-of-the-art MSDA methods on this multimodal data.

2. Related Work

(a) Multi-Source Domain Adaptation: MSDA techniques for image classification can be classified into discrepancy-based methods [17, 23] that reduce the domain shift by estimating the discrepancy between source and target domains. [17], generate the target pseudo-labels by creating clusters for each class; the initialization will depend on the source domains. Contrastive learning [17, 30] methods focus on minimizing the disparity within the same class while maximizing with the opposite classes. Adversarial learning [22, 48], and self-supervised [6, 36] approaches, which train different classifiers for each source while generating pseudo-labels from the classifier agreement to adapt to the target domain. Recently, Zeeshan et al. [45] proposed a subject-based MSDA method for recognition expression that considers subjects as domains to tackle many sources (up to 77) for the adaptation process. Even though there are advancements in MSDA, they all depend on unimodal (visual) modality, which leads us to introduce multimodality in the MSDA setting for subject-based ER.

(b) Multimodal Expression Recognition: Multimodal ER is widely explored in the literature. Praveen et al. [26] proposed a cross-attention method that fused multiple modalities for expression recognition. Aslam et al. [1] presented an LUPi paradigm that learns from multiple modalities but uses only a single modality at the time of inference. Similarly, in [2], the author presented an optimal transport knowledge distilling method from different modalities. Multimodal methods also receive attention in domain adaptation for EEG and eye movement signals. Wang et al. [39] presented a variational autoencoder (VAE) multimodal method leveraging cycle consistency and adversarial learning losses to reduce the shift between domains and overcome the modality separation problem. Likewise, in [15], they adapt a model by reducing the discrepancy (CORAL loss [33]) between source and target distributions while adding an intra-inter domain loss for modality alignment for a cross-subject expression recognition using multimodal EEG signals. This paper exploits multiple modalities (visual and physiological) in MSDA for adapting to a new, unlabeled target subject.

(c) Disentanglement in Expression Recognition: Dis-

entanglement methods have been used in ER to suppress identity or pose information that interferes with ER. Jiang and Deng [14] proposed a GAN-based model with separate encoders for expression, identity, and pose, followed by a decoder and discriminator to guide expression reconstruction. Xie et al. [42] introduced TDGAN, which fuses identity from one image and expression from another. While effective for visual data, these GAN-based approaches rely on image reconstruction, making them unsuitable for non-visual modalities like physiological signals, where such reconstruction is not meaningful. Pichler et al. [24] proposed a KNIFE method that disentangled the information by estimating and minimizing the entropy between two estimators. Motivated by this strategy, our MuSACo adopts a similar formulation to decouple identity- and expression-specific representations.

(d) Co-training for Domain Adaptation: Co-training is a well-established semi-supervised and unsupervised learning approach [3] that is used in many applications, such as semantic segmentation [9, 41], task decomposition [44], or in image classification [5]. It typically trains the model with modalities to produce more reliable pseudo-labels (PLs), while domain adaptation usually trains the model with a single modality that incorporates multiple classifiers to account for different views. Chen et al. [5] propose a method that introduces two different classifiers trained with different features controlled via a weighting mechanism while generating target pseudo-labels from the most confident classifier. MuSACo introduces a co-training method for multimodal data for the selection of source subjects. In addition, we select target confident PLs based on multiple classifiers trained on different modalities.

3. Proposed MuSACo Approach

MuSACo seeks to leverage complementary information from multiple modalities within MSDA using co-training to improve target personalization. This is accomplished through a two-step training process. Firstly, the non-discriminative identity information is disentangled from the source subjects while training task-specific backbones using source supervision. This ensures that only discriminative features are retained for recognizing the expression. Second, a co-training strategy is employed to select the most relevant source subjects for the target. For each source-target pair, similarity scores are computed from each modality. Sources that produce high similarity scores in either modality are selected, and a threshold (τ_{ss}) is applied to filter out less relevant sources. Exploiting the trained backbones, we generate target PLs through co-training. The modality with the highest confidence in its prediction is chosen, and the samples are considered reliable if their confidence exceeds a threshold (τ_{pl}). For domain alignment, class-aware alignment is performed on the target samples

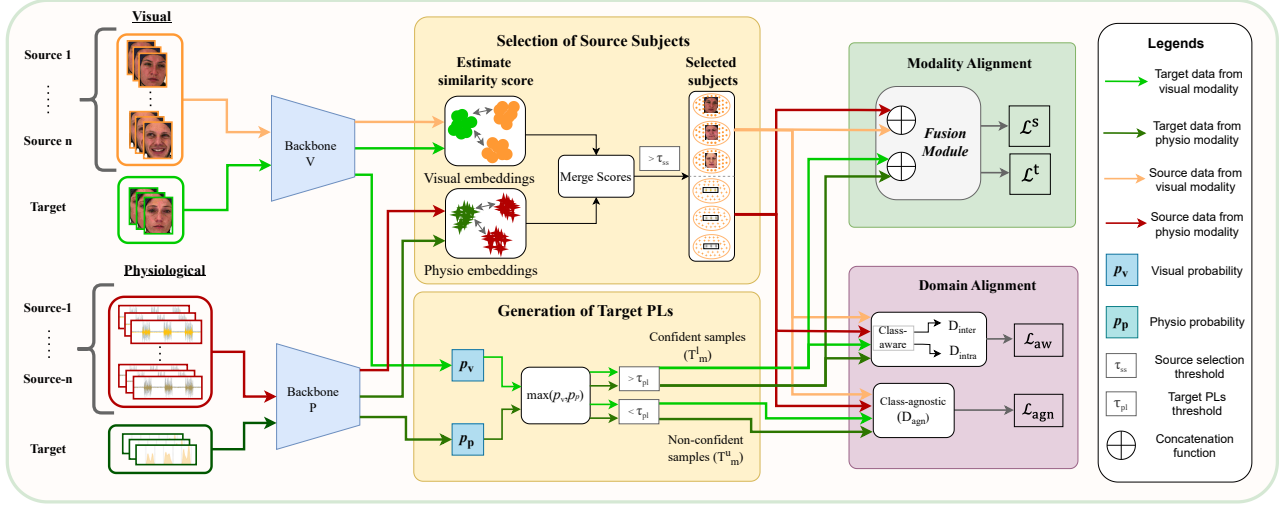


Figure 2. An overview of MuSACo shown in the particular case of $M = 2$ modalities (with visual + physiological). First, the similarity between source and target subjects is estimated using the **Selection of Source Subjects** module, followed by selecting the modality that gives the maximum probability score based on the threshold. Then, **Domain Alignment** is achieved by the **Generation of Target PLS** module through co-training. It calculates class-aware loss for each modality, combined with class-agnostic loss to learn from the non-confident target samples. Finally, the **Fusion Module** is introduced for the **Modality Alignment** through feature concatenation.

selected using τ_{pl} and class-agnostic alignment using non-confident samples. Finally, for modality alignment, features are concatenated from different modalities for every selected source and target subject, which are used to train the fusion module. MuSACo is illustrated in Fig.2.

3.1. Model Architecture

A multimodal multi-source expression classification task is considered, where a model is trained using several labeled source subjects $\mathcal{S}_m = \{\mathbf{S}_{m_1}, \dots, \mathbf{S}_{m_a}, \dots, \mathbf{S}_{m_D}\}$ and a single unlabeled target subject \mathbf{T}_m , where m is the number of modalities and $a = \{1, \dots, D\}$ is the number of source subjects. In MuSACo, without loss of generality, we consider two modalities: **visual** (v) and **physiological** (p), where $m \in \{v, p\}$. Each source \mathbf{S}_{m_a} contains N^s labeled samples $\{(\mathbf{x}_{m_j}^s, y_{m_j}^s, \hat{y}_{m_j}^s) | 1 \leq j \leq N^s\}$, where $y_{m_j}^s$ represents expression labels and $\hat{y}_{m_j}^s$ represents identity labels. We also define expression classes as $c = \{1, \dots, C\}$. The unlabeled target consists of N^t samples $\{\mathbf{x}_{m_j}^t | 1 \leq j \leq N^t\}$. **Backbones** are defined as $\mathcal{B} = \{B_1, \dots, B_M\}$, where each B belongs to its respective modality. Accordingly, we consider two backbones that correspond to B_v (visual) and B_p (physiological) modalities. It takes input from \mathbf{x}_m^s and \mathbf{x}_m^t and return embeddings of source $\mathbf{h}_m^s = \mathbf{h}_v^s, \mathbf{h}_p^s$ and target $\mathbf{h}_m^t = \mathbf{h}_v^t, \mathbf{h}_p^t$. Finally, the **fusion module** F is a two-layer perceptron that takes input extracted from \mathcal{S}_m and \mathbf{T}_m to perform feature fusion for the alignment of modalities.

3.2. Training Backbones with Disentanglement

Two backbones are trained for each modality – visual B_v and physiological B_p – using multiple labeled source subjects \mathcal{S}_m . To learn expression-discriminative representations, each modality is supervised using a cross-entropy loss:

$$\mathcal{L}_m^s = \frac{1}{D} \frac{1}{N^s} \sum_{i=1}^D \sum_{j=1}^{N^s} \text{CE}(\mathbf{y}_{m_j}^i, f_m(\mathbf{h}_{m_j}^i)) \quad (1)$$

where $\mathbf{h}_{m_j}^i$ is the embedding from modality m , $\mathbf{y}_{m_j}^i$ is the ground-truth expression label, and f_m is the modality-specific expression classifier. The loss \mathcal{L}_m^s is computed independently for each modality to ensure effective learning of modality-specific features.

Disentangled Identity-Information. Our approach is inspired by KNIFE [24], a differentiable entropy estimator, to disentangle identity information from expression-relevant features in each modality. We estimate the marginal entropy $H(\mathbf{h}_{m_j}^s)$ and the conditional entropy $H(\mathbf{h}_{m_j}^s | \hat{\mathbf{y}}_{m_j}^s)$. For each sample in the source subjects, the identity labels $\hat{y}_{m_j}^s$ are converted into one-hot representations $\hat{\mathbf{y}}_{m_j}^s \in R^k$ and define the disentanglement loss as:

$$\mathcal{L}_m^d = H(\mathbf{h}_{m_j}^s) + H(\mathbf{h}_{m_j}^s | \hat{\mathbf{y}}_{m_j}^s). \quad (2)$$

The classification loss \mathcal{L}_m^s and disentanglement loss \mathcal{L}_m^d are jointly optimized to preserve task-relevant features while removing identity information³.

³More details are provided in Section 2 of the supplementary material.

3.3. Domain Adaptation via Co-training

(a) Selection of Source Subjects. Selecting the most relevant source subjects from \mathcal{S}_m is a critical step in MuSACo method, where the model is trained on diverse sources to ensure robustness. However, when adapting to a target subject \mathbf{T}_m captured in a specific environment and cultural context (e.g., an adult Caucasian male), the source subjects must align with these characteristics to ensure effective adaptation. To address this, we leverage our multimodal system to define selection criteria based on **co-training**, which ensures that the chosen sources are highly relevant to the target subject. Given two modalities *visual* and *physiological*, estimate the cosine similarity between \mathcal{S} and \mathbf{T} using embeddings \mathbf{h}_m^s and \mathbf{h}_m^t ,

$$\mathbf{Q}_m(\mathcal{S}, \mathbf{T}) = \frac{\mathbf{h}_m^s \cdot \mathbf{h}_m^t}{\|\mathbf{h}_m^s\|_2 \cdot \|\mathbf{h}_m^t\|_2} \quad (3)$$

where $\|\cdot\|$ is the euclidean norm calculated for \mathbf{h}_m^s and \mathbf{h}_m^t . $\mathbf{Q}_m(\mathcal{S}, \mathbf{T})$ is estimated for each source and target pairs as,

$$P_m = [\mathbf{Q}_m^c(\mathbf{S}_{m_1}, \mathbf{T}_m), \dots, \mathbf{Q}_m^c(\mathbf{S}_{m_D}, \mathbf{T}_m)] \quad (4)$$

Here, P_m represents a dictionary list containing all pairwise distances computed using cosine similarity for each modality. Due to the distinct architectures of the modalities, such as a 2D CNN for the visual modality and a 1D CNN for the physiological modality, we normalize P_m to the range $[0, 1]$ to ensure comparability across modalities. We define P_v and P_p as the similarity scores for the visual and physiological modalities, respectively. These scores are merged into a combined set $\hat{P} = (P_v \cup P_p)$, from which we select source subjects whose distances exceed a predefined threshold τ_{ss} . The selection process is formalized as:

$$\tilde{\mathcal{S}}_m = \{\mathcal{S}_{m_i} : \hat{P}_i > \tau_{ss}\} \quad \forall i \in \{1, \dots, D\} \quad (5)$$

The selected source subjects for each modality form a subset $\tilde{\mathcal{S}}_m$, where $\tilde{\mathcal{S}}_m \subseteq \mathcal{S}_m$. This selection process ensures that only the most relevant source subjects are used for the target adaptation.

(b) Generation of Target Pseudo-Labels (PLs). In MSDA, reliable PLs determine the performance of a model on an unseen target subject [45]. MuSACo benefits from the multimodal by selecting confident target PLs using co-training. Given two backbones, B_v and B_p . We introduce samples \mathbf{x}_m^t from \mathbf{T}_m to produce softmax probabilities with respect to each modality, $p_v = \sigma(\mathbf{h}_v^s)$ and $p_p = \sigma(\mathbf{h}_p^s)$, taking the maximum probability $\hat{p} = \max(p_v, p_p)$ and applying a predetermined threshold τ_{pl} to select the confident samples, defined as:

$$\mathbf{T}_m^l = \{(\hat{x}_{m_j}, \hat{y}_{m_j}) | \hat{p} > \tau_{pl}, j \in \{1 \leq j \leq N^t\}\} \quad (6)$$

where \mathbf{T}_m^l represents the set of confident target samples for m modalities, we also store the confident classes $C =$

$\{y_i | (x_i, y_i) \in \mathbf{T}_m^l\}$. To differentiate between confident and non-confident samples, we create \mathbf{T}_m^u , defined as:

$$\mathbf{T}_m^u = \{(x_{m_j}) | \hat{p} \leq \tau_{pl}, j \in \{1 \leq j \leq N^t\}\} \quad (7)$$

where \mathbf{T}_m^u , defined the *non-confident* target samples, for the estimation of class-agnostic alignment (Section 3.3).

(c) Class-Aware Domain Alignment. We exploit class information to perform intra-class and inter-class alignment across domains. For intra-class alignment, samples from the same class are encouraged to reside in the same distribution space. Conversely, for inter-class alignment, samples from different classes are pushed further apart in the feature space. Class-aware alignment is computed using maximum mean discrepancy (MMD) [31], a statistical measure for estimating the disparity between two distributions. To sample out examples from the same class, we perform class-aware sampling on source and target subjects. The classes that belong to \mathbf{T}_m^l were denoted as \tilde{C} . We sample out examples from every subject belonging to multiple labeled sources. In each mini-batch, examples from every source and target are extracted for the same class. The intra-class discrepancy is defined as:

$$D_{\text{ita}}(\tilde{\mathcal{S}}_m, \mathbf{T}_m^l) = \frac{1}{D} \frac{1}{\tilde{C}} \sum_{a=1}^D \sum_{c=1}^{\tilde{C}} \text{MMD}(\mathbf{h}_{\mathbf{m}_a}^c, \mathbf{h}_m^c) \quad (8)$$

where, $\mathbf{h}_{\mathbf{m}_a}^c$ extracts features from each source subject, \mathbf{h}_m^c are the features extracted from the target subject, and \tilde{C} are the confident expression classes. Inter-class is defined as:

$$D_{\text{itr}}(\tilde{\mathcal{S}}_m, \mathbf{T}_m^l) = \frac{1}{D} \frac{1}{\tilde{C}(\tilde{C}-1)} \sum_{a=1}^D \sum_{c=1}^{\tilde{C}} \sum_{\substack{\hat{c}=1 \\ \hat{c} \neq c}}^{\tilde{C}} \text{MMD}(\mathbf{h}_{\mathbf{m}_a}^c, \mathbf{h}_m^{\hat{c}}) \quad (9)$$

where MMD is computed from the opposite classes \hat{c} for every source with the target. Alignment loss is estimated for every modality (*visual* and *physio*), ensuring that source and target align in their respective distribution space.

(d) Class-Agnostic Domain Alignment. Most MSDA methods [17, 30] employ class-aware alignment to bridge dissimilar distributions, often relying on PLs for the target subject. However, these pseudo-labels are prone to noise, and while denoising techniques have been proposed [6, 28, 30, 43], they typically use pre-determined thresholds to retain only the most confident pseudo-labels (CPL). This reliance on thresholds can limit performance, especially in ER, where subtle expressions may lead to discarding useful but less confident samples. To address this, a domain-agnostic loss is introduced that aligns non-confident samples to ensure that all target samples contribute to the adaptation process. This approach maximizes the utilization of available data for improving the target adaptation. The domain agnostic loss is defined as:

$$D_{\text{agn}}(\tilde{\mathcal{S}}_m, \mathbf{T}_m^u) = \frac{1}{D} \sum_{a=1}^D \text{MMD}(\mathbf{h}_{\mathbf{m}_a}^s, \mathbf{h}_m^t) \quad (10)$$

where $\mathbf{h}_{m_a}^s$ is the feature vector extracted from $\tilde{\mathcal{S}}_m$ subjects that contain samples not belong to $\tilde{\mathcal{C}}$. The total alignment loss for both modalities is calculated as:

$$\mathcal{L}_{\text{agn}} = D_{\text{agn}}(\tilde{\mathcal{S}}_v, \mathbf{T}_v^u) + D_{\text{agn}}(\tilde{\mathcal{S}}_p, \mathbf{T}_p^u) \quad (11)$$

$$\mathcal{L}_{\text{aw}} = [D_{\text{ita}}(\tilde{\mathcal{S}}_v, \mathbf{T}_v^l) - D_{\text{itr}}(\tilde{\mathcal{S}}_v, \mathbf{T}_v^l)] + [D_{\text{ita}}(\tilde{\mathcal{S}}_p, \mathbf{T}_p^l) - D_{\text{itr}}(\tilde{\mathcal{S}}_p, \mathbf{T}_p^l)] \quad (12)$$

where \mathcal{L}_{agn} and \mathcal{L}_{aw} are class-agnostic and class-aware losses respectively. For each modality, the intra-class and class-agnostic discrepancy is minimized, while the inter-class discrepancy is maximized.

(e) Modality Alignment. In multimodal settings, aligning modalities by adding a fusion network has proven to be very successful in enhancing model performance [1, 26]. In MuSACo method, to align the modalities, a fusion module F is introduced that projects the combined modality embeddings into a shared feature space. To train F for multiple source subjects, we use the embeddings \mathbf{h}_v^s and \mathbf{h}_p^s to perform feature concatenation $\mathbf{h}^s = \mathbf{h}_v^s \oplus \mathbf{h}_p^s$, and pass through F to calculate a cross-entropy loss:

$$\mathcal{L}^s = \frac{1}{D} \frac{1}{N^s} \sum_{i=1}^D \sum_{j=1}^{N^s} \text{CE}(\mathbf{y}_j^i, F(\mathbf{h}_j^i)) \quad (13)$$

where D is the source subject that contains the N^s number of samples. Modality alignment is estimated for each $\tilde{\mathcal{S}}$ and \mathbf{T} subject individually. We only calculated for the confident samples for the target \mathbf{T}_m^l , the embeddings are extracted \mathbf{h}_v^t and \mathbf{h}_p^t , and applied concatenation function $\mathbf{h}^t = \mathbf{h}_v^t \oplus \mathbf{h}_p^t$, then F is applied to calculate the cross-entropy loss:

$$\mathcal{L}_{\text{unsup}}^t = \frac{1}{N_l^t} \sum_{j=1}^{N_l^t} \text{CE}(\hat{\mathbf{y}}_j, F(\mathbf{h}_j^t)) \quad (14)$$

where N_l^t is the total number of reliable samples, and $\hat{\mathbf{y}}_j$ is the CPL. The final objective is to jointly optimize all four losses $\mathcal{L} = \mathcal{L}^s + \gamma \mathcal{L}_{\text{unsup}}^t + \alpha \mathcal{L}_{\text{agn}} + \beta \mathcal{L}_{\text{aw}}$, where γ , α , and β hyper-parameters weight the contribution of each loss.

4. Results and Discussion

4.1. Experimental Protocol

Datasets. All the methods were evaluated on two challenging multimodal ER datasets for subject-based adaptation. **Biovid Heat Pain (PartA)** [38] dataset consists of 87 subjects with 5 classes, corresponding to BL (no pain) and four pain intensity levels from PA-1 to PA-4. MuSACo follows the same protocol as [45] to consider 77 subjects as sources and 10 subjects as targets. **StressID** [4] dataset comprised 65 subjects taken in a lab-controlled environment. Due to the unavailability of certain modalities in 11 of the participants, our method considers 54 individuals, which includes

both modalities (visual and physiological), from which 44 source and 10 target subjects are selected. More details are provided in the supplementary material. In both datasets, visual and physiological (EDA) modalities are considered in all of our experiments.

Implementation Detail. In addition to the visual modality, the physiological modality, specifically electrodermal activity (EDA), is incorporated for both the BioVid and StressID datasets. For visual, ResNet18 [12] is used, following the same protocol as [45]. The images are resized to 100×100 resolution. For the physiological modality, an LSTM-based 1D-CNN network is included, consisting of two convolutional layers, one LSTM layer, and one fully connected layer. In addition, the expression head is constructed using 2-MLP layers. A batch size of 32 for the target subject, and the model is trained for 20 epochs. All the target subjects are split into train/val/test sets, and all the results are reported using a target test set. To select the confident target samples, τ_{pl} is set to 0.95. For selection of source subjects, τ_{ss} is set to 0.55 (Sec. 4.4-b).

Baseline Methods. The reported results correspond to the top-1% multimodal target accuracy across all target subjects. The evaluation begins with the **Lower Bound**, where a model is trained solely on labeled source subjects (77 for BioVid, 44 for StressID) and directly evaluated on the target test set without any target supervision. Results are reported for *visual-only*, *physio-only*, and *fusion* (vision + physio) modalities. Next, the **MM-UDA (blending)** setting blends all the source subjects into a single domain, then adapts to the unlabeled target subject using various UDA techniques, including DANN [8], CDAN [21], MMD [31], and MuSACo (UDA), which only use co-training to generate target pseudo-labels. Furthermore, MuSACo (MSDA) is compared against **MM-MSDA** approaches, including *CAN* [17], *Sub-based MSDA*, and *CMSDA* [30]. In all methods, a 1D-CNN-LSTM network is added for the physiological modality to ensure a fair comparison with our proposed approach. Finally, results for an *Upper Bound* setting are reported, where models are fine-tuned using labeled multimodal data from the target subject.

4.2. Comparison with State-of-the-Art Methods

Tab. 1 shows results on the **BioVid** dataset. All domain adaptation approaches outperform the lower-bound baselines (visual and both), confirming the effectiveness of multimodal domain adaptation in the context of pain estimation. Notably, the *Physio-only* baseline outperforms many standard UDA and MSDA methods, achieving an average accuracy of 34.5%. This reflects findings in prior work [2, 37, 40], where physiological signals are shown to be strong indicators of pain intensity, especially in subtle expression settings where visual cues are often weak or ambiguous. In contrast, the *Visual-only* baseline performs

Settings	Methods	Target Subjects										
		Sub-1	Sub-2	Sub-3	Sub-4	Sub-5	Sub-6	Sub-7	Sub-8	Sub-9	Sub-10	Avg
Lower Bound	Visual-only	37.1	27.2	26.3	29.6	28.4	28.6	35.6	22.1	33.6	19.7	28.8
	Physio-only	41.3	33.2	40.3	34.2	33.4	31.2	37.3	33.9	35.6	25.2	34.5
	Fusion	39.1	35.2	28.6	25.6	39.2	36.6	44.5	27.8	28.8	20.1	32.5
MM-UDA (Blending)	DANN [8]	39.4	28.4	31.5	33.4	37.6	31.5	34.2	26.6	34.3	27.4	32.4
	CDAN [21]	32.6	24.1	29.2	32.1	29.6	26.8	28.4	23.6	23.4	22.6	27.2
	MMD [31]	34.1	26.3	31.5	36.7	34.2	33.5	43.4	34.1	28.6	31.2	33.3
	MuSACo (UDA)	43.5	29.9	37.6	38.2	40.0	22.3	38.6	40.0	47.6	25.8	36.3
MM-MSDA	CAN [17]	43.2	32.2	27.2	33.6	33.4	32.5	36.6	32.4	41.5	33.8	34.6
	Sub-based _{top-k} [45]	43.5	42.2	28.5	22.5	29.1	32.5	40.6	41.2	38.0	28.4	34.6
	CMSDA [30]	39.4	39.4	29.4	36.6	39.2	39.1	38.4	35.7	45.2	25.6	36.8
	MuSACo (MSDA)	49.2	43.3	47.3	38.2	40.1	44.3	46.4	45.2	50.0	34.3	43.8
Upper Bound	Fine-tuning	83.6	78.5	70.0	71.6	71.5	64.5	76.8	76.9	78.5	64.8	73.6

Table 1. Accuracy of MuSACo with baselines against multimodal UDA, and MSDA methods on BioVid adapted to unlabeled data from 10 target subjects, Sub-1, ..., Sub-10. (Note that MM: Multimodal, L: Labeled and U: Unlabeled.)

Settings	Methods	Target Subjects										
		Sub-1	Sub-2	Sub-3	Sub-4	Sub-5	Sub-6	Sub-7	Sub-8	Sub-9	Sub-10	Avg
Lower Bound	Visual-only	71.1	23.2	51.4	63.3	55.6	63.2	72.7	48.7	60.0	59.6	56.8
	Physio-only	57.7	81.1	60.0	28.2	60.0	69.7	84.2	51.1	34.6	29.7	55.6
	Fusion	68.3	30.4	54.2	57.6	65.3	67.8	79.7	48.6	61.2	59.4	59.2
MM-UDA (Blending)	DANN [8]	65.3	65.3	73.3	66.4	67.3	72.3	73.2	55.3	70.4	57.2	66.6
	CDAN [21]	58.1	68.1	72.6	59.9	67.9	70.7	76.4	59.5	60.3	49.4	64.2
	MMD [31]	66.3	52.3	71.6	74.5	71.9	74.5	81.2	57.2	68.4	57.2	67.5
	MuSACo (UDA)	71.2	53.4	69.7	70.0	73.5	68.7	82.4	60.0	72.7	61.2	68.2
MM-MSDA	CAN [17]	69.3	81.2	67.2	59.3	62.3	74.2	83.3	60.0	66.8	59.3	68.2
	Sub-based _{top-k} [45]	70.8	74.9	73.6	70.6	59.8	77.9	71.8	49.9	63.9	69.8	68.3
	MuSACo (MSDA)	71.2	81.2	73.6	74.6	73.5	78.5	86.3	60.0	79.2	71.5	74.9
Upper Bound	Fine-tuning	83.4	84.5	98.2	98.1	89.7	87.6	90.0	89.6	89.4	95.7	90.6

Table 2. Accuracy of MuSACo with baselines, multimodal UDA and MSDA methods on StressID adapted to 10 unlabeled target subjects.

significantly worse (28.8%), and the naïve fusion of both modalities (without adaptation) does not exceed the performance of using physiological data alone. Among all methods, our approach achieves the highest overall performance. MuSACo (UDA) outperforms both the *lower-bound* and *UDA* baselines and is competitive with MSDA methods. Further, MuSACo (MSDA) achieves even better results, with a 9.3% gain over *physio-only* and 7.5% over MuSACo (UDA). It also outperforms MSDA baselines, with an average gain of 9.2% over CAN [17] and Sub-based_{top-k} [45], and 7% over CMSDA [30]. This shows our method effectively exploits modality complementarity, adapting to subject-specific signals in subtle pain recognition. Tab. 2 presents the performance on the **StressID** dataset. As expected, training without adaptation (lower bound) yields significantly lower accuracy across most subjects. Notably, fusing both modalities in the lower bound produces more stable performance compared to using either modality alone. This is due to the complementary nature of the modalities; when the visual modality underperforms, the physiological input often compensates, result-

ing in more balanced performance across subjects. Among existing methods, CAN achieves the highest performance on Sub-2, 8, whereas Sub-based_{top-k} gains the performance on Sub-3 that is comparable with our method. MuSACo (UDA) improved the performance on 3 out of 10 subjects while, on average, attaining a similar performance as MSDA methods. MuSACo (MSDA) outperformed every other method on all target subjects, with an overall gain of 15.7% from *lower-bound (both)*, 7.4% from MMD, 6.7% from MuSACo (UDA) and CAN, and 6.6% from Sub-based MSDA.

4.3. Visualizations

In Fig. 3 (left), t-SNE [35] shows how different methods separate class embeddings. The source-only model yields noisy, overlapping features. Subject-based MSDA [45] improves clustering but struggles with overlaps (e.g., PA3 in PA4). In contrast, MuSACo better clusters same-class samples and separates opposing ones. Fig. 3 (right) shows the closest and furthest source subjects to a target (Sub-10, BioVid), based on similarity scores from visual and physi-

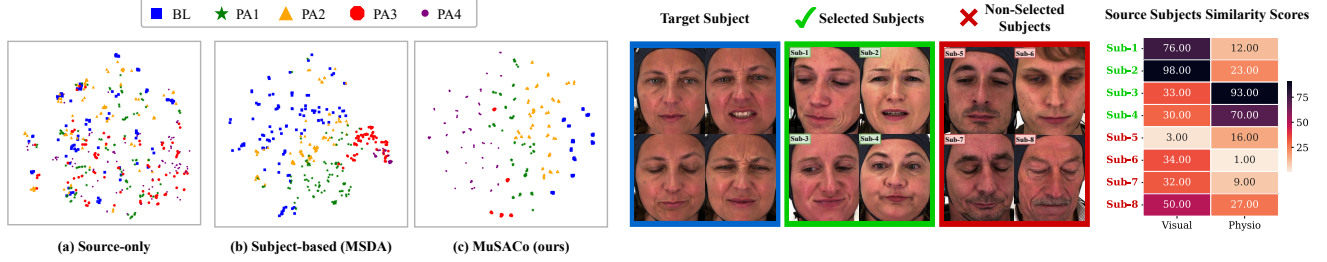


Figure 3. **Left:** t-SNE visualizations. The source-only produced indistinguishable feature class clusters. Sub-based MSDA [45] reduces some noise by separating classes to some extent. MuSACo creates more separable clusters for each class. **Right:** Visualization of selected and non-selected source subjects for a reference target subject, with similarity scores from visual and physiological modalities.

ological modalities. A source is selected if either modality exceeds the threshold τ_{ss} , e.g., *Sub-1/2* (visual) and *Sub-3/4* (physio). *Sub-5* to *Sub-8* are excluded as both scores fall below τ_{ss} (see Sec. 4.4(b) for threshold selection).

4.4. Ablation Studies

(a) Impact of difference loss components. To evaluate the contribution of each loss component, an incremental ablation study is conducted by gradually introducing loss terms. As shown in Tab. 3, adding the unsupervised target loss \mathcal{L}^t significantly improves accuracy over the source-only baseline. Further gains are achieved by incorporating the class-agnostic loss \mathcal{L}_{agn} and the class-aware loss \mathcal{L}_{aw} , both of which contribute to improving the adaptation process in the absence of target labels. The combination of all loss terms achieves the highest accuracy of 40.7%.

(b) Impact of selection of source subjects threshold. As shown in Fig. 4, setting $\tau_{ss} = 0$ disables the source selection mechanism, including all source subjects (77 for Biovid), achieving an average accuracy of 37.6%. As τ_{ss} increases, fewer but more relevant source subjects are selected based on similarity scores, improving performance. The best accuracy of 39.8% is achieved at $\tau_{ss} = 0.55$, where only 21 source subjects are selected on average. This demonstrates the effectiveness of co-training in identifying complementary and informative sources for improved target adaptation. A breakdown of subject-wise selection of each target subject are provided in the suppl. material.

\mathcal{L}^s	\mathcal{L}^t	\mathcal{L}_{agn}	\mathcal{L}_{aw}	Acc
✓				32.1
✓	✓			36.5
✓	✓	✓		37.2
✓	✓		✓	38.0
✓	✓	✓	✓	40.7

Table 3. Impact of individual loss components.

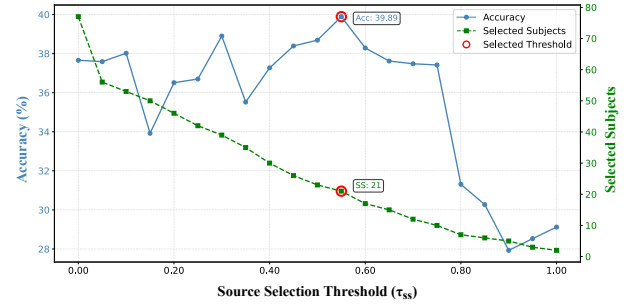


Figure 4. Source subject threshold (τ_{ss}) selection based on the accuracy. The red circle highlights the selected $\tau_{ss} = 0.55$.

5. Conclusion

Domain adaptation methods typically focus on individual modalities, or in the case of multimodal MSDA, they aggregate data from all source subjects, losing critical subject-specific cues necessary for effective adaptation to unlabeled target data. In this paper, MuSACo, a multimodal subject-specific MSDA is introduced that effectively leverages subject-level information for a personalized adaptation. In particular, MuSACo selects the most similar source subjects based on multimodal similarity and applies co-training to generate pseudo-labels for the target. Class-aware and class-agnostic losses are combined to leverage both confident and uncertain target samples effectively. Final alignment is achieved via feature concatenation across modalities. MuSACo is validated on challenging MER datasets and shows consistent gains over baselines, UDA (blending), and MSDA methods. MuSACo supports personalized modeling by adapting to each target subject through relevant sources, making it well-suited for health-related applications, where subject-specific cues are crucial. While the current method requires training a separate model per target subject, future work will explore lightweight or continual adaptation approaches to reduce retraining overhead and enable faster subject-specific adaptation.

6. Supplementary

6.1. Algorithm

(a) **Selection of Subject-Specific Sources.** Algorithm 1 shows the subject-specific selection of source subjects with co-training. Given source subjects \mathcal{S} and specific target subject \mathbf{T} , extracted features using visual B_v and physiological B_p encoders. Construct a similarity metric z^v and z^p by measuring CosineSimilarity between every source subject and target. To estimate the maximum score, we normalize the similarities, merge them, and sort them in descending order, followed by a threshold that selects the most relevant subjects from the target.

Algorithm 1 Subject-Specific Selection of Source Subjects

Require:

\mathcal{S} : labeled source subjects, \mathbf{T} : unlabeled target domain,
 B_{vis} : visual encoder, B_{phy} : physio encoder, τ_{ss} : threshold
to select relevant source subjects

- 1: **Initialize:** $\mathbf{z}^v \leftarrow \emptyset, \mathbf{z}^p \leftarrow \emptyset$
 - 2: Decompose \mathbf{T} into \mathbf{T}^v and \mathbf{T}^p
 - 3: **# Extract target features**
 - 4: $\mathbf{X}_t^v \leftarrow B_{vis}(\mathbf{T}^v), \mathbf{X}_t^p \leftarrow B_{phy}(\mathbf{T}^p)$
 - 5: **for** each domain $\mathbf{S}_i \in \mathcal{S}$ **do**
 - 6: Decompose \mathbf{S}_i into \mathbf{S}^v and \mathbf{S}^p
 - 7: **# Extract source features**
 - 8: $\mathbf{X}_s^v \leftarrow B_{vis}(\mathbf{S}^v), \mathbf{X}_s^p \leftarrow B_{phy}(\mathbf{S}^p)$
 - 9: **# Compute similarities**
 - 10: $z_i^v \leftarrow \cos(\mathbf{X}_s^v, \mathbf{X}_t^v)$
 - 11: $z_i^p \leftarrow \cos(\mathbf{X}_s^p, \mathbf{X}_t^p)$
 - 12: **# Append similarities**
 - 13: $\mathbf{z}^v \leftarrow \mathbf{z}^v \cup z_i^v, \mathbf{z}^p \leftarrow \mathbf{z}^p \cup z_i^p$
 - 14: **end for**
 - 15: $\mathbf{z}^v \leftarrow \text{norm}(\mathbf{z}^v), \mathbf{z}^p \leftarrow \text{norm}(\mathbf{z}^p)$
 - 16: Merge similarities: $\mathbf{z} \leftarrow \text{merge}(\mathbf{z}^v, \mathbf{z}^p)$
 - 17: Sort \mathbf{z} in descending order
 - 18: Select relevant sources : $\tilde{\mathcal{S}} \leftarrow \tau_{ss}(\mathbf{z})$
-

(b) **Training Protocol of MuSACo.** In algorithm 2, we show our training protocol of adapting to an unlabeled target subject. All the equation numbers referenced here correspond to those in the main paper.

6.2. Hyperparameters

Training of backbones. momentum=0.9, weight decay=5e-4, stochastic gradient descent (SGD) optimizer [29], learning rate=1e-4 with lr scheduler (eta_min=0.00002). **Weighting parameters.** In MuSACo, we give different weights to different loss functions. For the contribution of class-agnostic loss $\gamma = 0.5$, and for class-aware loss $\alpha = 0.1$. **Disentanglement.** Knife is very sensitive to hyperparameters; we have explored several parameters to make it work with the

Algorithm 2 Training protocol of MSACo

Require:

$\tilde{\mathcal{S}}$: selected labeled source subjects

\mathbf{T} : unlabeled target domain

- 1: **for** epoch **do**
 - 2: Perform co-training on \mathbf{T} to generate pseudo-labels (after every n epochs)
 - 3: **for** iteration **do**
 - 4: **# Class-aware alignment**
 - 5: Class-aware domain sampling of $\tilde{\mathcal{S}}$ and \mathbf{T}
 - 6: Estimate intra-class discrepancy using (Eq: 8)
 - 7: Estimate inter-class discrepancy using (Eq: 9)
 - 8: Compute class-aware loss \mathcal{L}_{aw} (Eq: 12)
 - 9: **# Domain-agnostic alignment**
 - 10: Domain-agnostic sampling of $\tilde{\mathcal{S}}$ and \mathbf{T}
 - 11: Estimate domain agnostic using (Eq 10)
 - 12: Compute domain-agnostic loss \mathcal{L}_{agn} (Eq: 11)
 - 13: **# Modality alignment**
 - 14: Perform feat concatenation of source subjects between modalities \mathbf{h}_v^s and \mathbf{h}_p^s
 - 15: Perform feat concatenation of target subject between modalities \mathbf{h}_v^t and \mathbf{h}_p^t
 - 16: Compute modality align loss \mathcal{L}^s using (Eq: 13)
 - 17: Compute modality align \mathcal{L}_{unsup}^t using (Eq: 14)
 - 18: **end for**
 - 19: **end for**
-

expression recognition task. The most critical parameters that is selected for our experiments are: zd_dim=1024, zc_dim=77, hidden_state=512, layers=3, nb_mixture=10, with learning-rate=0.01.

6.3. Detail on Training the Source Backbones

Training of the source backbones (visual and physiological) involves disentangling the identity-related features from the expression task. Our method is inspired by KNIFE[24], a fully differentiable entropy estimator, which we adapted for disentanglement in a multi-modal framework. The KNIFE estimator optimizes the backbones (visual and physiological) by decoupling non-task-related information through individual modality-specific gradient-based optimization. We leverage the KNIFE estimator to minimize the mutual information between modalities in eliminating identity features and enhancing the disentanglement of task-relevant features across distributions. We first estimate the marginal entropy of embedding \mathbf{h}_m^s as,

$$H(\mathbf{h}_m^s) = -\mathbb{E}[MMp(\mathbf{h}_m^s)] \quad (15)$$

where \mathbb{E} is the expectation over the distribution \mathbf{h}_m^s and $p(\cdot)$ is the probability density. To estimate the conditional entropy between the features and identities, For each sample

in the source subjects, we convert the identity labels $\hat{y}_{m_j}^s$ into one-hot representations $\hat{Y}_{m_j}^s \in R^k$. Then, conditional entropy is calculated as,

$$H(\mathbf{h}_{m_j}^s | \hat{Y}_{m_j}^s) = -\mathbb{E}[\log p(\mathbf{h}_{m_j}^s | \hat{Y}_{m_j}^s)] \quad (16)$$

where $p(\cdot, \cdot)$ is the conditional probability density between features $\mathbf{h}_{m_j}^s$ and prediction $\hat{Y}_{m_j}^s$. The total learning loss is calculated as:

$$\mathcal{L}_m^d = H(\mathbf{h}_m^s) + H(\mathbf{h}_{m_j}^s | \hat{Y}_{m_j}^s). \quad (17)$$

By minimizing \mathcal{L}_m^d , the model is encouraged to decouple the information associated with \hat{y}_m^s from the feature embeddings \mathbf{h}_m^s . Furthermore, we introduce a fixed Identity-head I_m head composed of two fully connected layers. It takes embeddings \mathbf{h}_m^s without gradient backpropagation. I_m works as a regularizer in conjunction with disentanglement loss to suppress non-discriminative identity-related information during target adaptation. The disentanglement loss decouples identity-related information, while the I_m helps to constrain redundant (non-task-specific) features, ensuring the model focuses on learning relevant expression-related representations.

6.4. Datasets

Biovid Heat Pain [38] dataset consists of 87 subjects captured in a controlled environment. It consists of five classes, including: *No-Pain*, *PA-1*, *PA-2*, *PA-3*, and *PA-4*. Every individual recorded 20 videos per class, corresponding to 100 videos per subject. We follow the same protocol as [40], where it eliminates the initial 2 seconds from the video, which does not show any spike indicating pain. In our experiment, we follow [45] to consider 77 subjects as sources and 10 subjects as targets: Sub-1 (081014_w_27), Sub-2 (101609_m_36), Sub-3 (112009_w_43), Sub-4 (091809_w_43), Sub-5 (071309_w_21), Sub-6 (073114_m_25), Sub-7 (080314_w_25), Sub-8 (073109_w_28), Sub-9 (100909_w_65), Sub-10 (081609_w_40). **StressID** [4] dataset comprised 65 (47 men and 18 women) subjects taken in a lab-controlled environment. Each participant was exposed to 11 tasks, grouped into 4 categories: watching emotional videos, breathing, interactive tasks, and relaxation. These tasks were captured using three different modalities (visual, physiological, and audio). Due to the unavailability of certain modalities in 11 of the participants, we only consider 54 individuals, which includes all the modalities. In our experiments, we take 44 subjects as sources and 10 subjects as targets. The target subject selection follows a 70% (men) and 30% (women) ratio, reflecting the higher number of male participants in the dataset. For each participant, there are up to 11 task-specific videos, from which we extracted frames at 1

Subjects	ID	Gender	NSV	SV	No. frames
Sub-1	kycf	Men	5	6	1021
Sub-2	uymz	Men	8	3	880
Sub-3	h8s1	Men	4	7	957
Sub-4	ctzy	Men	2	9	1041
Sub-5	p9i3	Men	5	6	1041
Sub-6	7h5u	Men	5	5	917
Sub-7	g7r2	Men	8	3	1041
Sub-8	b9w0	Women	4	7	1026
Sub-9	r3zm	Women	3	8	909
Sub-10	x1q3	Women	2	9	1001

Table 4. StressID target subject demographics and total number of samples (NSV: No Stress Videos, SV: Stress Videos)

fps for per-image expression classification. Tab. 4 shows the selected target subject demographics (ID, Gender) and the total number of samples.

6.5. Ablation

(a) Impact of Weighting Hyperparameters. We performed a sequential weight sensitivity analysis for the key loss terms, \mathcal{L}_{unsup}^t , \mathcal{L}_{aw} , and \mathcal{L}_{agn} shown in Tab. 5). First, we varied the weight of the target PL loss while keeping the others fixed at 1. Using the best result, we tuned the class-aware alignment loss, followed by the class-agnostic loss, each time fixing the previously selected best weights. This approach highlights the individual contribution of each loss to overall performance.

Weight	Accuracy		
	\mathcal{L}_{unsup}^t	\mathcal{L}_{aw}	\mathcal{L}_{agn}
0.01	38.6	40.7	40.9
0.05	40.5	40.7	43.8
0.1*	40.3	43.9	41.4
0.3	39.9	39.9	40.1
0.5*	38.7	40.3	44.1
0.7	39.9	39.9	39.9
0.9	40.2	41.4	43.9
1*	40.7	40.7	40.9
2	40.6	39.6	41.9
5	40.2	38.8	22.0

Table 5. Ablation study on loss weights. Each loss weight is varied while keeping the previously selected optimal weights fixed.

(b) Ablation on Target PLs Threshold (τ_{pl}). We conducted an ablation to select a target PLs threshold (τ_{pl}) value as shown in the Tab. 7. We found that $\tau_{pl} = 0.95$ produced the best trade-off, balancing label quality with sample

τ_{ss}	Sub-1	Sub-2	Sub-3	Sub-4	Sub-5	Sub-6	Sub-7	Sub-8	Sub-9	Sub-10	Avg SS	Avg Acc
0.00	77	77	77	77	77	77	77	77	77	77	77.0	37.66
0.05	56	55	62	52	57	50	59	53	52	65	56.1	37.59
0.10	53	50	57	52	53	48	57	52	49	63	53.4	38.02
0.15	50	47	56	49	49	45	52	50	44	61	50.3	33.92
0.20	48	44	50	47	45	43	48	44	40	54	46.3	36.51
0.25	43	39	44	44	45	43	41	40	35	51	42.5	36.70
0.30	39	35	40	37	43	41	37	38	33	49	39.2	38.90
0.35	35	28	34	35	38	36	32	36	29	44	34.7	35.52
0.40	31	22	28	32	35	33	30	28	27	39	30.5	37.27
0.45	31	20	26	26	31	30	25	20	21	35	26.5	38.39
0.50	26	16	24	26	28	26	21	16	18	34	23.5	38.69
0.55	20	23	23	24	22	23	16	13	15	30	20.9	39.89
0.60	16	15	21	20	15	18	16	10	12	27	17.0	38.29
0.65	12	13	20	19	15	16	11	11	10	22	14.9	37.62
0.70	9	8	15	15	12	15	7	6	9	21	11.7	37.48
0.75	7	6	13	12	10	13	5	5	8	20	9.9	37.42
0.80	5	5	9	7	6	11	3	4	8	16	7.4	31.31
0.85	4	4	6	7	5	9	3	3	5	13	5.9	30.27
0.90	2	2	6	6	4	7	3	3	3	10	4.6	27.93
0.95	2	2	4	3	3	3	2	2	3	5	2.9	28.53
1.00	2	2	2	2	2	2	2	2	2	2	2.0	29.12

Table 6. Number of selected subjects (SS) for each target subject across different τ_{ss} thresholds. Lower τ_{ss} values indicate fewer selected sources. We also report the average number of selected subjects and the corresponding average accuracy.

quantity. To mitigate the issue of excluding useful but uncertain samples when using a high threshold, we introduce a domain-agnostic loss that ensures the model will also learn from the non-confident samples. Note that target ground-truth labels were used for this analysis to evaluate the effectiveness of pseudo-labels.

Threshold (τ_{pl})	Accuracy
0.50	40.2
0.60	48.1
0.70	44.7
0.75	46.5
0.80	46.2
0.85	48.6
0.90	46.7
0.95	52.0

Table 7. Accuracy at different pseudo-label confidence thresholds (τ_{pl})

(c) Source Subject Selection Analysis Tab. 6 shows the number of selected source subjects for each of the 10 target subjects for the Biovid dataset for various threshold (τ_{ss}) values. As τ_{ss} increases, fewer source subjects are selected, reducing potential noise from irrelevant domains. Notably, the accuracy improves when transitioning from $\tau = 0$ to

Exp-head	Id-head	Knife	Visual	Physio
✓			25.1	36.2
✓		✓	26.3	37.0
✓	✓	✓	28.3	38.2

Table 8. Ablation on disentanglement module for visual and physiological modalities for Biovid dataset.

moderate thresholds (e.g., $\tau_{ss} = 0.45$ or 0.55), demonstrating that selective inclusion of source data benefits generalization. The best average accuracy of 39.89% is achieved with $\tau_{ss} = 0.55$, using approximately 21 subjects on average.

(d) Computational Complexity To analyze the time complexity, we evaluated all methods under identical conditions using a ResNet-18 backbone (11.7M parameters), a fixed batch size of 32, and the same GPU (NVIDIA A100-SXM4-40GB). The reported training time includes both source and target, and inference time with accuracy are summarized in Tab. 9. The significant training time of CAN [17] is due to its design, which processes each source domain separately and performs class-wise contrastive learning between each source and the target domain within every batch. While manageable for benchmark datasets like Office-31 (3 domains), this becomes prohibitively expensive when scaling

to our subject-based adaptation setting, where the number of source domains averages over 30, resulting in 19,625 ms of target training time. In contrast, our method retrieves class-wise samples from all source domains and from the target domain, then performs a single contrastive operation per batch, significantly reducing overhead. It completes target training in just 426 ms ($46\times$ faster than CAN) while improving accuracy from 34.6% to 43.8%. Although CMSDA [30] and sub-based [45] adaptation methods are more efficient (271 ms and 234 ms), they fail to yield improvements in accuracy. Results show that our method offers the best trade-off between efficiency and accuracy, with inference time similar to other baselines.

Method	Src Train	Trg Train	Inf	Acc
CAN	59	19,625	8.03	34.6
Sub-based	59	234	7.36	34.6
CMSDA	—	271	4.07	36.8
Ours (all srcs)	59	1895	7.82	39.3
Ours (co-train)	59	426	7.64	43.8

Table 9. Training and inference time (per batch) of our proposed and baseline methods. All times are shown in ms.

6.6. MuSACo

MuSACo (inspired by the layered harmony of Musaca) integrates two synergistic modules for subject-specific adaptation: a co-training-based source subject selection module that identifies the most relevant sources using complementary cues from multiple modalities, and an adaptation module that aligns source and target domains using class-aware and class-agnostic losses. Like Musaca’s layered composition—where distinct elements work in harmony—MuSACo leverages modality-specific strengths to guide pseudo-label generation and fuse information effectively. This enables robust, personalized adaptation for each target subject while maintaining consistency across modalities.

References

- [1] Muhammad Haseeb Aslam, Muhammad Osama Zeeshan, Marco Pedersoli, Alessandro L. Koerich, Simon Bacon, and Eric Granger. Privileged knowledge distillation for dimensional emotion recognition in the wild. In *Proceedings of the IEEE/CVF conference on computer vision and pattern recognition*, pages 3338–3347, 2023. 1, 2, 3, 6
- [2] Muhammad Haseeb Aslam, Muhammad Osama Zeeshan, Soufiane Belharbi, Marco Pedersoli, Alessandro Lameiras Koerich, Simon Bacon, and Eric Granger. Distilling privileged multimodal information for expression recognition using optimal transport. In *18th International Conference on Automatic Face and Gesture Recognition (FG)*, pages 1–10, 2024. 1, 3, 6
- [3] Avrim Blum and Tom Mitchell. Combining labeled and unlabeled data with co-training. In *Proceedings of the eleventh annual conference on Computational learning theory*, pages 92–100, 1998. 3
- [4] Hava Chaptoukaev, Valeriya Strizhkova, Michele Panariello, Bianca Dalpaos, Aglind Reka, Valeria Manera, Susanne Thümmel, Esma Ismailova, Massimiliano Todisco, Maria A Zuluaga, et al. Stressid: a multimodal dataset for stress identification. *Advances in Neural Information Processing Systems*, 36:29798–29811, 2023. 6, 10
- [5] Minmin Chen, Kilian Q Weinberger, and John Blitzer. Co-training for domain adaptation. *Advances in neural information processing systems*, 24, 2011. 3
- [6] Zhongying Deng, Da Li, Yi-Zhe Song, and Tao Xiang. Robust target training for multi-source domain adaptation. *CoRR*, 2022. 3, 5
- [7] Andrius Dzedzickis, Artūras Kaklauskas, and Vytautas Bucinskas. Human emotion recognition: Review of sensors and methods. *Sensors*, 20(3):592, 2020. 2
- [8] Yaroslav Ganin, Evgeniya Ustinova, Hana Ajakan, Pascal Germain, Hugo Larochelle, François Laviolette, Mario March, and Victor Lempitsky. Domain-adversarial training of neural networks. *Journal of machine learning research*, 17(59):1–35, 2016. 6, 7
- [9] Jose L Gómez, Gabriel Villalonga, and Antonio M López. Co-training for unsupervised domain adaptation of semantic segmentation models. *Sensors*, 23(2):621, 2023. 3
- [10] Arthur Gretton, Karsten M Borgwardt, Malte J Rasch, Bernhard Schölkopf, and Alexander Smola. A kernel two-sample test. *The Journal of Machine Learning Research*, 13(1):723–773, 2012. 1
- [11] Jing Han, Lun Xie, Jing Liu, and Xue Li. Personalized broad learning system for facial expression. *Multimedia Tools and Applications*, 79(23):16627–16644, 2020. 1
- [12] Kaiming He, Xiangyu Zhang, Shaoqing Ren, and Jian Sun. Deep residual learning for image recognition. In *Proceedings of the IEEE conference on computer vision and pattern recognition*, pages 770–778, Piscataway, USA, 2016. IEEE. 6
- [13] Rachael E Jack, Caroline Blais, Christoph Scheepers, Philippe G Schyns, and Roberto Caldara. Cultural confusions show that facial expressions are not universal. *Current biology*, 19(18):1543–1548, 2009. 1
- [14] Jing Jiang and Weihong Deng. Disentangling identity and pose for facial expression recognition. *IEEE Transactions on Affective Computing*, 13(4):1868–1878, 2022. 3
- [15] Magdiel Jiménez-Guarneros and Gibran Fuentes-Pineda. Cfda-csf: A multi-modal domain adaptation method for cross-subject emotion recognition. *IEEE Transactions on Affective Computing*, 15(3):1502–1513, 2024. 2, 3
- [16] Magdiel Jiménez-Guarneros, Gibran Fuentes-Pineda, and Jonas Grande-Barreto. Mmda: A multimodal and multisource domain adaptation method for cross-subject emotion recognition from eeg and eye movement signals. *IEEE Transactions on Computational Social Systems*, 2024. 2
- [17] Guoliang Kang, Lu Jiang, Yunchao Wei, Yi Yang, and Alexander Hauptmann. Contrastive adaptation network for

- single-and multi-source domain adaptation. *IEEE transactions on pattern analysis and machine intelligence*, 44(4): 1793–1804, 2020. 2, 3, 5, 6, 7, 11
- [18] Shan Li and Weihong Deng. Deep emotion transfer network for cross-database facial expression recognition. In *2018 24th International Conference on Pattern Recognition (ICPR)*, pages 3092–3099, Piscataway, USA, 2018. IEEE. 1
- [19] Wei Liu, Jie-Lin Qiu, Wei-Long Zheng, and Bao-Liang Lu. Comparing recognition performance and robustness of multimodal deep learning models for multimodal emotion recognition. *IEEE Transactions on Cognitive and Developmental Systems*, 14(2):715–729, 2021. 1
- [20] Mingsheng Long, Han Zhu, Jianmin Wang, and Michael I Jordan. Unsupervised domain adaptation with residual transfer networks. *Advances in neural information processing systems*, 29, 2016. 1
- [21] Mingsheng Long, Zhangjie Cao, Jianmin Wang, and Michael I Jordan. Conditional adversarial domain adaptation. *Advances in neural information processing systems*, 31, 2018. 6, 7
- [22] Van-Anh Nguyen, Tuan Nguyen, Trung Le, Quan Hung Tran, and Dinh Phung. Stem: An approach to multi-source domain adaptation with guarantees. In *Proceedings of the IEEE/CVF International Conference on Computer Vision*, pages 9352–9363, Piscataway, USA, 2021. IEEE. 3
- [23] Xingchao Peng, Qinxun Bai, Xide Xia, Zijun Huang, Kate Saenko, and Bo Wang. Moment matching for multi-source domain adaptation. In *Proceedings of the IEEE/CVF international conference on computer vision*, pages 1406–1415, Piscataway, USA, 2019. IEEE. 3
- [24] Georg Pichler, Pierre Jean A Colombo, Malik Boudiaf, Günther Koliander, and Pablo Piantanida. A differential entropy estimator for training neural networks. In *International Conference on Machine Learning*, pages 17691–17715. PMLR, PMLR, 2022. 3, 4, 9
- [25] R Gnana Praveen, Eric Granger, and Patrick Cardinal. Deep weakly supervised domain adaptation for pain localization in videos. In *2020 15th IEEE International Conference on Automatic Face and Gesture Recognition (FG 2020)*, pages 473–480. IEEE, 2020. 1
- [26] R Gnana Praveen, Wheidima Carneiro de Melo, Nasib Ullah, Haseeb Aslam, Osama Zeeshan, Théo Denorme, Marco Pedersoli, Alessandro L Koerich, Simon Bacon, Patrick Cardinal, et al. A joint cross-attention model for audio-visual fusion in dimensional emotion recognition. In *Proceedings of the IEEE/CVF conference on computer vision and pattern recognition*, pages 2486–2495, 2022. 1, 2, 3, 6
- [27] Gnana Praveen Rajasekhar, Eric Granger, and Patrick Cardinal. Deep domain adaptation with ordinal regression for pain assessment using weakly-labeled videos. *Image and Vision Computing*, 110:104167, 2021. 1
- [28] Chuan-Xian Ren, Yong-Hui Liu, Xi-Wen Zhang, and Ke-Kun Huang. Multi-source unsupervised domain adaptation via pseudo target domain. *IEEE Transactions on Image Processing*, 31:2122–2135, 2022. 5
- [29] Sebastian Ruder. An overview of gradient descent optimization algorithms. *arXiv preprint arXiv:1609.04747*, 2016. 9
- [30] Marin Scalbert, Maria Vakalopoulou, and Florent Couzinié-Devy. Multi-source domain adaptation via supervised contrastive learning and confident consistency regularization. *arXiv preprint arXiv:2106.16093*, 2021. 2, 3, 5, 6, 7, 12
- [31] Dino Sejdinovic, Bharath Sriperumbudur, Arthur Gretton, and Kenji Fukumizu. Equivalence of distance-based and rkhs-based statistics in hypothesis testing. *The annals of statistics*, pages 2263–2291, 2013. 5, 6, 7
- [32] Masoumeh Sharafi, Emma Ollivier, Muhammad Osama Zeeshan, Soufiane Belharbi, Marco Pedersoli, Alessandro Lameiras Koerich, Simon Bacon, et al. Disentangled source-free personalization for facial expression recognition with neutral target data. *arXiv preprint arXiv:2503.20771*, 2025. 1
- [33] Baochen Sun and Kate Saenko. Deep coral: Correlation alignment for deep domain adaptation. In *European conference on computer vision*, pages 443–450. Springer, 2016. 3
- [34] Panagiotis Tzirakis, George Trigeorgis, Mihalalis A Nicolaou, Björn W Schuller, and Stefanos Zafeiriou. End-to-end multimodal emotion recognition using deep neural networks. *IEEE Journal of selected topics in signal processing*, 11(8): 1301–1309, 2017. 1, 2
- [35] Laurens Van der Maaten and Geoffrey Hinton. Visualizing data using t-sne. *Journal of machine learning research*, 9 (11), 2008. 7
- [36] Naveen Venkat, Jogendra Nath Kundu, Durgesh Singh, Ambareesh Revanur, et al. Your classifier can secretly suffice multi-source domain adaptation. *Advances in Neural Information Processing Systems*, 33:4647–4659, 2020. 3
- [37] Paul Waligora, Muhammad Haseeb Aslam, Muhammad Osama Zeeshan, Soufiane Belharbi, Alessandro Lameiras Koerich, Marco Pedersoli, Simon Bacon, and Eric Granger. Joint multimodal transformer for emotion recognition in the wild. In *Proceedings of the IEEE/CVF Conference on Computer Vision and Pattern Recognition*, pages 4625–4635, 2024. 1, 6
- [38] Steffen Walter, Sascha Gruss, Hagen Ehleiter, Junwen Tan, Harald C Traue, Philipp Werner, Ayoub Al-Hamadi, Stephen Crawcour, Adriano O Andrade, and Gustavo Moreira da Silva. The biovid heat pain database data for the advancement and systematic validation of an automated pain recognition system. In *2013 IEEE international conference on cybernetics (CYBCO)*, pages 128–131. IEEE, 2013. 6, 10
- [39] Yixin Wang, Shuang Qiu, Dan Li, Changde Du, Bao-Liang Lu, and Huiguang He. Multi-modal domain adaptation variational autoencoder for eeg-based emotion recognition. *IEEE/CAA Journal of Automatica Sinica*, 9(9):1612–1626, 2022. 2, 3
- [40] Philipp Werner, Ayoub Al-Hamadi, and Steffen Walter. Analysis of facial expressiveness during experimentally induced heat pain. In *2017 Seventh international conference on affective computing and intelligent interaction workshops and demos (ACIIW)*, pages 176–180. IEEE, 2017. 6, 10
- [41] Yingda Xia, Dong Yang, Zhiding Yu, Fengze Liu, Jinzheng Cai, Lequan Yu, Zhuotun Zhu, Daguang Xu, Alan Yuille, and Holger Roth. Uncertainty-aware multi-view co-training

for semi-supervised medical image segmentation and domain adaptation. *Medical image analysis*, 65:101766, 2020. [3](#)

- [42] Siyue Xie, Haifeng Hu, and Yizhen Chen. Facial expression recognition with two-branch disentangled generative adversarial network. *IEEE Transactions on Circuits and Systems for Video Technology*, 31(6):2359–2371, 2020. [3](#)
- [43] Ruijia Xu, Ziliang Chen, Wangmeng Zuo, Junjie Yan, and Liang Lin. Deep cocktail network: Multi-source unsupervised domain adaptation with category shift. In *Proceedings of the IEEE conference on computer vision and pattern recognition*, pages 3964–3973, 2018. [1](#), [5](#)
- [44] Luyu Yang, Yan Wang, Mingfei Gao, Abhinav Shrivastava, Kilian Q Weinberger, Wei-Lun Chao, and Ser-Nam Lim. Deep co-training with task decomposition for semi-supervised domain adaptation. In *Proceedings of the IEEE/CVF international conference on computer vision*, pages 8906–8916, 2021. [3](#)
- [45] Muhammad Osama Zeeshan, Muhammad Haseeb Aslam, Soufiane Belharbi, Alessandro Lameiras Koerich, Marco Pedersoli, Simon Bacon, and Eric Granger. Subject-based domain adaptation for facial expression recognition. In *2024 IEEE 18th International Conference on Automatic Face and Gesture Recognition (FG)*, pages 1–10. IEEE, 2024. [1](#), [2](#), [3](#), [5](#), [6](#), [7](#), [8](#), [10](#), [12](#)
- [46] Muhammad Osama Zeeshan, Marco Pedersoli, Alessandro Lameiras Koerich, and Eric Grange. Progressive multi-source domain adaptation for personalized facial expression recognition. *arXiv preprint arXiv:2504.04252*, 2025. [1](#)
- [47] Jianhua Zhang, Zhong Yin, Peng Chen, and Stefano Nichele. Emotion recognition using multi-modal data and machine learning techniques: A tutorial and review. *Information Fusion*, 59:103–126, 2020. [1](#)
- [48] Sicheng Zhao, Bo Li, Pengfei Xu, Xiangyu Yue, Guiguang Ding, and Kurt Keutzer. Madan: multi-source adversarial domain aggregation network for domain adaptation. *International Journal of Computer Vision*, 129(8):2399–2424, 2021. [3](#)
- [49] Ronghang Zhu, Gaoli Sang, and Qijun Zhao. Discriminative feature adaptation for cross-domain facial expression recognition. In *2016 International Conference on Biometrics (ICB)*, pages 1–7. IEEE, 2016. [1](#)